Flux pinning mechanisms in graphene doped MgB_2 superconductors

K. S. B. De Silva[a], X. Xu[a], S. Gambhir[b], X. L. Wang[a], W. X. Li[a], G. G. Wallace[b], S. X. Dou[a,*]

[a]*Institute for Superconducting and Electronic Materials, University of Wollongong, Northfields Avenue, Wollongong, New South Wales, 2522, Australia*

[b]*Intelligent Polymer Research Institute, University of Wollongong, Northfields Avenue, Wollongong, New South Wales, 2522, Australia*

*shi@uow.edu.au

The effects of graphene doping on the superconducting properties of MgB_2 were studied. We found that small addition of graphene significantly improves the superconducting properties of MgB_2, with only a small reduction in T_c. Low resistivity, high critical fields, and enhanced flux-flow activation energy were observed for the optimally doped bulk sample. The spatial fluctuation in the transition temperature (δT_c pinning) is the flux pinning mechanism in graphene doped MgB_2.

Key words: Electrical resistivity/ conductivity; Metallic superconductors; Magnetoresistance; Graphene doping

The discovery of superconductivity in MgB_2 at 39 K has attracted great interest around the world, due to its high critical temperature (T_c), which is the highest among the intermetallic superconductors [1]. Improvements in critical current density (J_c) in the presence of applied magnetic field, the upper critical field (H_{c2}), and the irreversibility field (H_{irr}), have been key issues in MgB_2 superconductors, as the critical current density of pristine MgB_2 drops rapidly with increasing magnetic field, which is mainly due to its poor flux pinning and low H_{c2}. Carbon can be considered as the most successful dopant for enhancing H_{c2}, as it causes strong intraband electron scattering in the σ and π bands of B-B bonds [2-6]. However, the carbon

doping comes with its own drawback of reducing T_c, which limits the application temperature of MgB_2 [6].

Graphene is becoming recognized as a novel dopant for MgB_2, with its unique properties stemming from its semi-metallic nature [7]. The difference between the thermal expansion coefficients of graphene and MgB_2 could form of lattice defects which are capable of improving flux pinning [8]. However, whether superconducting properties can be improved by a small addition of graphene is still unclear, and therefore, the focus of this study is on improving our understanding of the microstructural changes that occur due to doping and their effects towards enhancing the superconducting properties of MgB_2.

Graphene doped bulk samples were prepared via the diffusion method from crystalline boron powder (0.2 to 2.4 μm) 99.999%, Mg ingot (99.84%), and highly reduced chemically converted graphene (rCCG) as precursors. Highly reduced chemically converted graphene (rCCG) was obtained by excessive reduction as reported by Dan Li et al.,[7]. The resulting rCCG agglomerates were further treated with thionyl chloride, as reported by Eda et al.,[9] to further improve the electrical conductivity.

Initially, boron and graphene powders were mixed by hand milling according to the formula $MgB_{2-x}C_x$, where x = 0, 1, and 5 mol % graphene. Powders were then pressed into pellets 13 mm in diameter and inserted into a soft iron tube with the stoichiometric ratio of Mg to B, plus 20% excess Mg to compensate for the loss of Mg during sintering. The samples were sintered at 800°C for 10 hours in a quartz tube at a heating rate of $5^o\,Cmin^{-1}$ under high purity argon (Ar 99.9%) gas.

The phase identification and crystal structure investigations were carried out using an X-ray diffractometer (GBCMMA) with Cu-Kα radiation (λ = 1.54059 Å). The Raman scattering was measured using a confocal laser Raman spectrometer (HORIBA Jobin Yvon system) with a 100× microscope. The SEM images were taken using Zeiss Ultra Plus scanning

electron microscope. The superconducting transition temperature, T_c, was determined from the AC susceptibility measurements, and the magnetic J_c was derived from the width of the magnetization loop using Bean's model [10] by a Physical Properties Measurement System (PPMS). The resistivity measurements were conducted using the standard dc four-probe technique under magnetic fields up to 13 T. The upper critical field (H_{c2}) and the irreversibility field (H_{irr}) were determined using the 90% and 10% criteria of R(T) for different applied fields, where R(T) is the normal state resistance near 40 K. The active cross-section (A_F) was calculated from the resistivity, ρ, using Rowell's model [11].

The room temperature X-ray diffraction patterns (XRD) of undoped and graphene (G) doped MgB_2 show all the Bragg reflections of the hexagonal MgB_2 structure. Table 1 shows the critical temperature, lattice parameters *a* and *c*, and full width at half maximum (FWHM) of the (110) diffraction peak values of undoped and G-doped MgB_2 bulk samples. Only a slight decrease in critical temperature is observed due to graphene doping. Even at the 5% doping level, T_c is decreased by just 1 K, which is not common with other carbon sources [3, 4]. The refinement results revealed that the *a*-parameter is slightly reduced with increasing doping level, which indicates that carbon is substituted into B sites [2]. Increased FWHM of the (110) diffraction peak for the graphene doped samples also gives evidence of strain effects that occurred due to graphene doping [12]. As chemical substitution can affect the crystal and electronic structure, as well as the degree of disorder, substitution can alter the phonon spectrum, by changing the phonon frequency and electron-phonon coupling strength [13]. There are three peaks observed for all the samples. The peak centred around 600 cm^{-1} arises from the E_{2g} phonon mode representing the in-plane B bond stretching, whereas the other two peaks represent the phonon density of states (PDOS) due to disorder. As evidenced by Figure 1a, a slight Raman shift to lower frequency near 600 cm^{-1} can be observed for the optimally doped sample (G 1%), which gives clear evidence of induced tensile strain in the 1%

graphene doped MgB_2 sample. However, as the doping level increases, the E_{2g} phonon peak shifts to the higher frequency side, which indicates that the weakening of the electron-phonon coupling by carbon substitution dominates the induced tensile strain effect [13]. Figure 1b, and 1c and 1d show the SEM images of the undoped, 1% G-doped and 5% G-doped samples respectively. It can be seen that graphene doped samples are highly dense, and with well connected grains than the undoped sample.

Figure 2a shows the in-field J_c performance at 5 and 20 K for undoped and graphene doped bulk samples. Critical current density curves for the doped samples show strong improvement over that of the undoped sample at 5 K. At the optimal doping level (graphene 1 mole %), there is nearly 43 times improvement compared to the undoped sample at 8 T, 5 K. The critical current density at high fields near H_{c2} is mainly governed by H_{c2}, hence higher H_{c2} leads to a higher J_c [14]. This, together with improved connectivity factor explains the reason for higher J_c observed in 1% G-doped samples at high fields. However, the optimal J_c value at high fields reported in this paper is lower than the one reported by Xu et al.,[8], owing to the difference in the experimental route, where, it was produced by boron powder which is ball milled in toluene medium with graphene. This also gives one reason for the difference of the optimal doping levels in each case. Furthermore, the graphene production routine is also influencing on the optimal doping level as it can vary the amount of carbon and oxygen remaining in the graphene. We believe both these reasons account for such a low optimal doping level in this study. At zero field, 20 K, all samples showed quite high critical current density values of more than 4.1×10^5 A/cm^2, and there was no J_c degradation observed at zero field for the doped samples. At zero field, all the defects act as point pinning centres and J_c linearly increased with H_{c2} [14]. The connectivity is also a major factor which governs the self-field J_c [15]. Therefore, the improvement in the critical current density at zero field at 20 K, can be attributed to improved connectivity and upper critical field due to graphene doping.

Figure 2b shows the normal state resistivity of undoped and graphene doped MgB_2 bulk samples. Although it is very common to show increased resistivity for MgB_2 doped samples, as the carbon doping reduces the electron mean free path, these samples showed a reduced resistivity after doping. However, the effective area factor appears to be more dominant in determining the resistivity of these MgB_2 samples. The active cross-sectional area (A_F) for undoped, 1% G-doped and 5% G-doped MgB_2 was 0.157, 0.250, and 0.19 respectively. The value A_F has increased due to graphene doping, which provides a clue to the reduction in resistivity. This improvement in the connectivity is confirmed by SEM images given in figure 1b, 1c and 1d. However, the improvement of A_F for the 5% G-doped MgB_2 is lesser than the 1% G-doped MgB_2, which reasons out the reduction of J_c performance of it, as the over doping tends to reduce the intergrain connectivity [11]. RRR, i.e., the ratio of the resistivity at 300 K to that at 40 K, reflects the degree of electron scattering. The RRR for undoped, 1% G-doped and 5% G-doped MgB_2 was 3.68, 2.81, and 2.87 respectively. When the electron scattering is high, it causes a reduction in the RRR values. The observed RRR values for the graphene doped samples are smaller than that of the pure sample, which is in a good agreement with the literature [11, 16].

It is well known that the core interaction, which is dominant in MgB_2, is described with two mechanisms named δT_c pinning and δl pinning. The δT_c pinning is caused by the spatial variation of the Ginzburg-Landau (GL) coefficient α associated with disorder in the T_c, and the δl pinning is caused by the variation of the charge-carrier mean free path *l* near lattice defects [17]. According to the model proposed by Qin et al.,[17], δT_c is the prominent pinning mechanism in pure MgB_2. Further, it defines that the crossover field, B_{sb}, as the field separating the single vortex regime from the regime where the vortices form small bundles, below which the J_c is almost independent of the applied field. (B_{sb} is taken as the field at

which the J_c drops by 5% compared to the J_c at zero field.) The variation of B_{sb} with reduced temperature ($t = T/T_c$) for δT_c and δl pinning is given by Eqs. (1) and (2), respectively:

$$B_{sb} = B_{sb}(0)\,[(1-t^2)/(1+t^2)]^{2/3} \quad (1)$$

$$B_{sb} = B_{sb}(0)\,[(1-t^2)/(1+t^2)]^{2} \quad (2)$$

As observed from Figure 3, the curve representing the δT_c pinning is in good agreement with measured data for the 1% G-doped sample, while the data for the 5% G-doped sample shows a slight variation from δT_c pinning behaviour, although it does not fit with δl pinning. Generally, carbon doped MgB_2 obeys δl pinning, owing to the increased scattering and hence, the reduced charge-carrier mean free path l near lattice defects [5, 18]. This again points out that graphene acts differently from other carbon sources when doped into the MgB_2 matrix.

Broadening of the resistive transition due to thermally activated flux flow (TAFF) in undoped and graphene doped bulk samples was studied in order to determine the relationship between the flux-flow energy barrier, U_0, and the applied magnetic field. The main mechanism of flux creep or flux flow in MgB_2 is the thermal activation of flux line motion over the energy barrier U_0 of the pinning centres, and this is indicated by a broadening of the resistive transition [19]. This broadening is explained in terms of a dissipation of the energy arising from the motion of vortices. Therefore, it is considered that the resistance in the low resistance region depends mainly on thermally activated flux flow, which is given by Eq. (3):

$$\rho(T, B) = \rho_0 \exp[-U_0/k_B T] \quad (3)$$

Here, U_0 is the flux-flow activation energy, which can be obtained from the slope of the linear part of the Arrhenius plot, ρ_0 is a field independent pre-exponential factor, and k_B is Boltzmann's constant [19]. Figure 4a shows the Arrhenius plot for 1% G-doped sample. All curves show linear behaviour at low temperature, which indicates that the dependence of U_0 is approximately linear at low temperature, and as the temperature goes up, it levels off at a field independent value which corresponds to the normal state resistivity [19]. As revealed in

Figure 4b, an enhanced value of U_0 can be seen for the G-doped samples in the low field region, especially at the optimum doping level. The field dependences of U_0 for all samples showed a weak relationship with increasing field up to B ≈ 4.5 T, where single-vortex pinning dominates. The undoped sample follows the power law $U_0 \propto B^{-0.98}$, whereas the power for 1% G-doped and 5% G-doped samples was around -0.75. The activation energy for all samples shows stronger field dependence at higher field, which is characteristic of collective creep [20]. However, the field dependence of U_0 for the undoped sample follows the power law $U_0 \propto B^{-5.4}$, whereas the powers for the 1% G-doped and 5% G-doped samples were -2.14 and -2.81 respectively, which indicates less field dependence of U_0 compared to the undoped sample.

In summary, a systematic study of the effects of graphene doping on the superconducting properties of MgB_2 has been conducted and improvements in superconducting properties, such as critical current density, and critical fields were observed due to graphene doping. Refinement results together with Raman analysis have shown that graphene doping leads to tensile strain in the MgB_2 lattice. We found that δT_c pinning is the flux pinning mechanism in graphene doped MgB_2. A noticeable enhancement in the flux-flow activation energy, U_0, was observed in graphene doped MgB_2 at low fields. All these improvements have positively affected on the enhancement of J_c, at the optimal doping level sample. Graphene is a novel and promising dopant for effectively enhancing the superconducting properties of MgB_2 without much reduction of T_c. Furthermore, we believe that graphene can also be used as a co-dopant for further enhancement in J_c performance.

This research was performed with the support of the Australian Research Council (ARC) through Project LP0989352. The authors would like to thank Dr. T. Silver, Dr. S. Zhou, Dr.

Y. Zhang, D. Attard, D. Wong and M. Shahbazi for their helpful discussions. This work was supported by Hyper Tech Research Inc., Oh, USA and the University of Wollongong.

[1] J. Nagamatsu, N. Nakagawa, T. Muranaka, Y. Zenitani, J. Akimitsu, Nature 410 (2001) 63-64.

[2] R. H. T. Wilke, S. L. Bud'ko, P. C. Canfield, D. K. Finnemore, R. J. Suplinskas, S. T. Hannahs, Phys. Rev. Lett. 92 (2004) 217003-4.

[3] A.Vajpayee, V. P. S. Awana, H. Kishan, A. V. Narlikar, G. L. Bhalla, X. L. Wang, J. Appl. Phys. 103 (2008) 07C708-3.

[4] C. Shekhar, R. Giri, R. S. Tiwari, O. N. Srivastava, S. K. Malik, J. Appl. Phys. 102 (2007) 093910-7.

[5] S. R. Ghorbani, X. L. Wang, S. X. Dou, Sung-IK Lee, M. S. A. Hossain, Phys. Rev. B 78 (2008) 184502-5.

[6] E. W.Collings, M. D. Sumption, M. Bhatia, M .A. Susner, S. D. Bohnenstiehl, Supercond. Sci. Technol. 21 (2008) 103001-15.

[7] D. Li, M. B. Muller, S. Gilje, R. B. Kaner, G. G. Wallace, Nat Nano 3 (2008) 101-105.

[8] X. Xu, S. X. Dou, X. L. Wang, J. H. Kim, M. Choucair, W. K. Yeoh, R. K. Zheng S. P. Ringer, Supercond. Sci. Technol. 23 (2010) 085003-8.

[9] G. Eda, Y. Y. Lin, S. Miller, C. W. Chen, W. F. Su, M. Chhowalla, Appl. Phys. Lett. 92 (2008) 233305-3.

[10] C. P. Bean, Rev. Mod. Phys. 36 (1964) 31-39.

[11] J. M. Rowell, Supercond. Sci. Technol. 16 (2003) R17-R27.

[12] J. H. Kim, S. X. Dou, J. L. Wang, D. Q. Shi, X. Xu, M. S. A. Hossain, W. K. Yeoh, S. Choi T. Kiyoshi, Supercond. Sci. Technol. 20 (2007) 448-451.

[13] W. X. Li, Y. Li, R. H. Chen, R. Zeng, S. X. Dou, M. Y. Zhu, H. M. Jin, Phys. Rev. B 77 (2008) 094517-7.

[14] Y. Zhang, X. Xu, Y. Zhao, J. H. Kim, C. Lu, S. H. Zhou, S. X. Dou, Supercond. Sci. Technol. 21 (2008) 115004-6.

[15] M. Eisterer, Supercond. Sci. and Technol. 20 **(**2007) R47- R73.

[16] X. L. Wang, S. X. Dou, M. S. A. Hossain, Z. X. Cheng, X. Z. Liao, S. R. Ghorbani, Q. W. Yao, J. H. Kim, T. Silver, Phys. Rev. B 81 (2010) 224514-6.

[17] M. J. Qin, X. L. Wang, H. K. Liu, S. X. Dou, Phys. Rev. B 65 (2002) 132508-4.

[18] J. L. Wang, R. Zeng, J. H. Kim, L. Lu, and S. X. Dou Phys. Rev. B **77** (2008) 174501-7

[19] A. Sidorenko, V. Zdravkov, V. Ryazanov, S. Horn, S. Klimm, R. Tidecks, A. Wixforth, T. Koch, T. Schimmel, Philosophical Magazine 85 (2005) 1783-90.

[20] J. Jaroszynski, F. Hunte, L. Balicas, Youn-Jung Jo, I. Raicevic, A. Gurevich, and D. C. Larbalestier, F. F. Balakirev, L. Fang, P. Cheng, Y. Jia, H. H. Wen, Phys. Rev. B 78 (2008) 174523-9.

TABLE 1. Lattice parameters and full width half maximum (FWHM) variation with doping level.

Graphene doping level (%)	T_c (K)	Lattice parameter *a* (Å)	Lattice parameter *c* (Å)	FWHM (110) (^{o})
0	38.9	3.086(1)	3.526(1)	0.335
1	38.3	3.085(1)	3.527(1)	0.480
5	37.9	3.083(1)	3.524(1)	0.400

Figures Captions:

Figure 1.(a). Raman spectra with Gaussian fitted E_{2g} mode and phonon density of states (PDOS) for undoped and graphene doped MgB_2. (b), (c) and (d) SEM images for undoped, 1% G-doped and 5% G-doped MgB_2 bulk samples respectively.

Figure 2. (a) Variation of the critical current density with applied magnetic field and (b) Variation of the resistivity with temperature for undoped and graphene doped MgB_2 bulk samples. Inset in (b) shows the variation of the normalized resistivity with temperature.

Figure 3. Temperature dependence of the cross over field B_{sb} for 1% graphene doped MgB_2 bulk sample (a) and 5% graphene doped MgB_2 bulk sample (b).

Figure 4. (a) Arrhenius plot for resistivity at different magnetic fields for 1% graphene doped MgB_2 bulk sample and (b) the dependence of the activation energy U_0/k_B on magnetic field for undoped and graphene doped MgB_2 bulk samples.

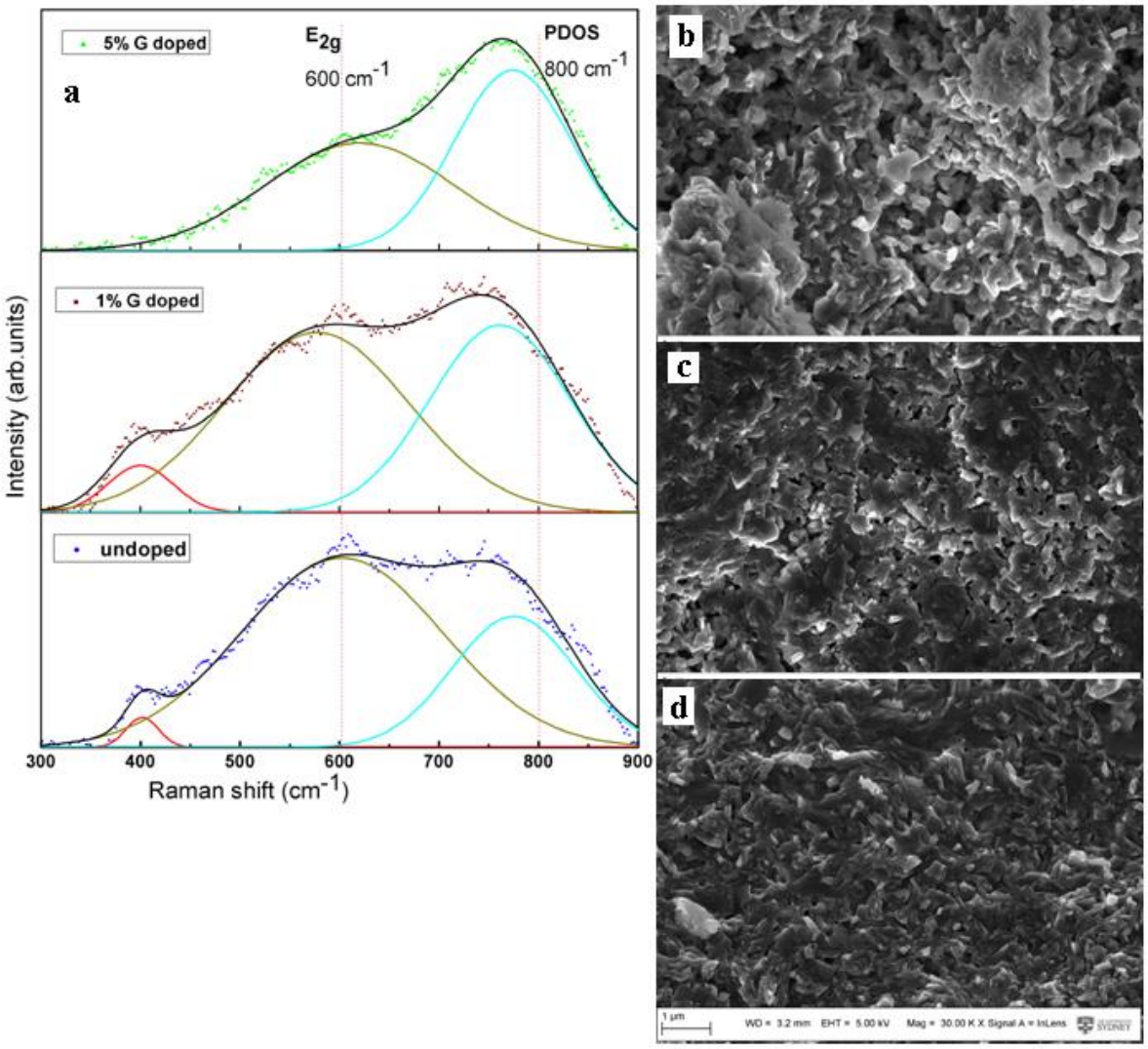
a
5% G doped
E_{2g}
600 cm^{-1}
PDOS
800 cm^{-1}
1% G doped
undoped
Intensity (arb.units)
Raman shift (cm^{-1})
300
400
500
600
700
800
900
b
c
d
1 µm
WD = 3.2 mm EHT = 5.00 kV Mag = 30.00 K X Signal A = InLens

Fig. 1

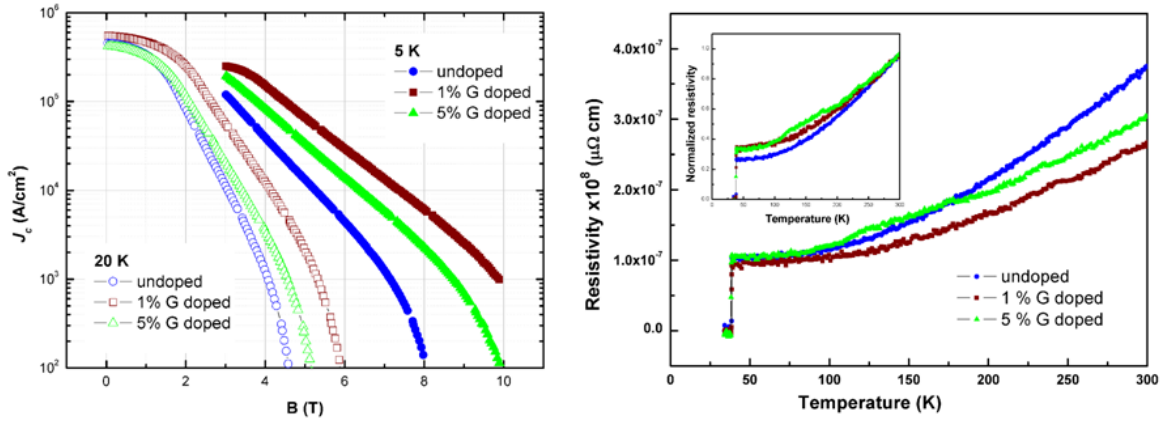
5 K
undoped
1% G doped
5% G doped
20 K
undoped
1% G doped
5% G doped
J_c (A/cm^2)
B (T)
Resistivity x10^8 (µΩ cm)
Normalized resistivity
Temperature (K)
undoped
1 % G doped
5 % G doped
Temperature (K)

Fig. 2

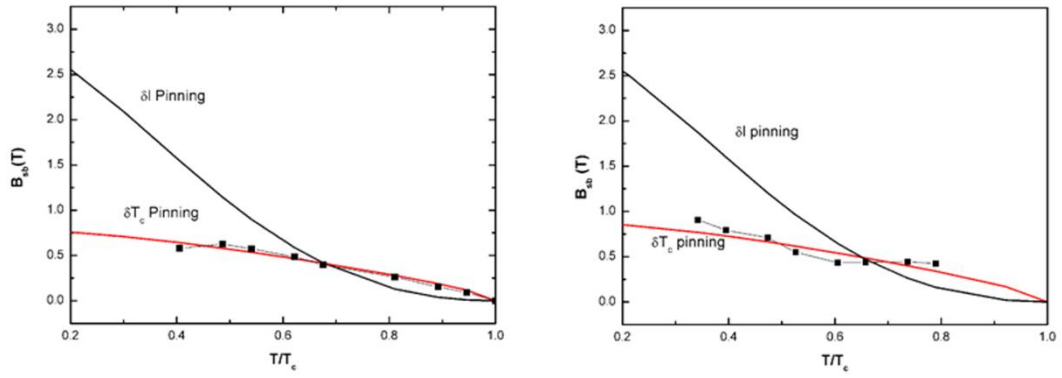
δl Pinning
δT$_c$ Pinning
B$_{sb}$(T)
T/T$_c$
δl pinning
δT$_c$ pinning
B$_{sb}$ (T)
T/T$_c$

Fig. 3

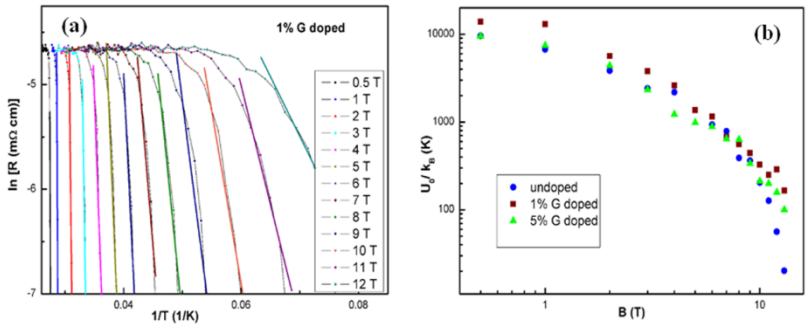
(a)
1% G doped
0.5 T
1 T
2 T
3 T
4 T
5 T
6 T
7 T
8 T
9 T
10 T
11 T
12 T
ln [R (mΩ cm)]
1/T (1/K)
(b)
undoped
1% G doped
5% G doped
U$_0$/ k$_B$ (K)
B (T)

Fig. 4